

Void nucleation at a sequentially plasma-activated silicon/silicon bonded interface

M M R Howlader, F Zhang and M G Kibria

Department of Electrical and Computer Engineering, McMaster University, 1280 Main Street West, Hamilton, ON L8S 4K1, Canada

E-mail: mrhowlader@ece.mcmaster.ca

Received 30 December 2009, in final form 20 March 2010

Published 11 May 2010

Online at stacks.iop.org/JMM/20/065012

Abstract

Two 4 inch silicon wafers were directly bonded using a sequentially plasma-activated bonding method (i.e. O₂ reactive ion etching (RIE) plasma followed by N₂ microwave (MW) radicals) at room temperature. The bonded wafers were annealed from 200 to 900 °C in order to explore the nucleation of voids at the interface. The plasma-induced void nucleation was dominated by O₂ RIE power over O₂ RIE activation time. The thermal-induced void nucleation occurred preferentially at the plasma-induced defect sites. The nucleation of void density was quantitatively determined and explained using high-resolution transmission electron microscopy observations. The electron energy loss spectroscopy results revealed the existence of silicon oxide at the bonded interface. The reduction in bonding strength after annealing at high temperature is correlated to the increase in void density. The contact angle and surface roughness of the sequentially plasma-treated surfaces have been observed to explain the nucleation of voids and the reduction of bonding strength. The plasma-induced defect sites such as nanopores and craters have been identified using an atomic force microscope.

(Some figures in this article are in colour only in the electronic version)

1. Introduction

A room temperature plasma-based bonding method called sequential plasma-activated bonding (SPAB) has been demonstrated for packaging of micro-electromechanical systems (MEMS), microfluidics and optoelectronic devices [1]. The SPAB combines the physical sputtering process of reactive ion etching (RIE) plasma with chemical reactivity of microwave (MW) radicals [2]. In the SPAB, spontaneous bonding occurs because of the concurrent removing of surface contaminants and native oxides, and depositing of oxides or nitrides on the activated surfaces. This process provides a high reactive surface that allows spontaneous bonding at room temperature [2]. The SPAB offers high bonding strength equivalent to the bulk materials without annealing.

One of the issues in SPAB is the voids or unbonded regions at the interface. Voids control the reliability of the bonded interface such as bonding strength and hermeticity. Voids mainly attribute to the presence of surface particles,

contaminants (i.e. hydrocarbon, metal ions from tweezers), reaction byproducts (i.e. H₂O and H₂) and plasma-induced defects. Nucleation of voids may accelerate during the fabrication process flow at higher temperatures in some applications. For example, in the smart-cut process to fabricate the silicon-on-insulator (SOI) substrate, ion implanted and bonded specimens go through the high temperature annealing step which is required for layer transfer [3]. Hence, the study on the nucleation of voids at the bonded interface under different processing conditions such as plasma parameters, annealing environment and temperature is needed.

Previously, the SPAB of silicon (Si) wafers showed that the bonding strengths were reduced after annealing at 300 and 600 °C in air [4]. The cause of the reduction of the bonding strength was believed to be due to the formation of voids and brittle oxide layers across the interface. While the quality (i.e. tensile strength) of the bonded interface was investigated after annealing at 300 and 600 °C, the cause of the reduction of bonding strength after annealing was not investigated in terms

Table 1. Plasma parameters used for silicon surface activation.

Specimen number	O ₂ RIE plasma			N ₂ MW radical		
	Power (W)	Time (s)	Pressure (Pa)	Power (W)	Time (s)	Pressure (pa)
A1	200	15	60	2500	30	60
A2		30				
A3		60				
B1	200	30	60	2500	15	60
B2	300					
B3	400					
C	300	30	60	–	–	–

of the void nucleation at the interface. In other study [5], Si/Si interfacial voids as a function of oxygen (O₂) RIE plasma and nitrogen (N₂) radical time and gas pressure showed that the number and size of the voids were increased as a function of O₂ RIE plasma time and gas pressure, but insignificant influence of N₂ radical time and pressure was evident. Also, the influence of O₂ RIE power in SPAB on the void nucleation has not been investigated yet.

This paper reports a systematic investigation of the void nucleation and a quantitative analysis of the void density at the Si/Si bonded interface using infrared (IR) transmission images as a function of O₂ RIE time, power and post-bonding annealing in air and nitrogen gas. The water contact angle and surface roughness of silicon have been observed in order to gain insights into the void nucleation and bonding strength of the high temperature-annealed Si/Si interface. Interfacial microstructural observation was performed using high-resolution transmission electron microscopy (HRTEM) and electron energy loss spectroscopy (EELS) measurements.

2. Experimental procedure

Commercially available one-side polished 4 inch (100 mm) Si (1 0 0) wafers were used. The thicknesses of the wafers were $525 \pm 25 \mu\text{m}$. The wafers were p-type and the resistivity was 20–30 $\Omega \text{ cm}$.

The sequential plasma activation of silicon surfaces was accomplished using a newly developed hybrid plasma bonding (HPB) system as shown in figure 1. The wafer level HPB system consists of plasma activation and anodic bonding chambers. For this study, only the plasma activation chamber was used. The plasma activation chamber is equipped with RIE and MW plasma sources. The plasma activation chamber is separated into top and bottom compartments by an ion trapping metallic plate. The RIE and MW plasmas were sequentially generated using O₂ and N₂ gases at the bottom and top compartments, respectively. The ion trapping metallic plate has 1 mm diameter holes, which trap charged ions. Therefore, MW plasma generates electrically neutral ions at the bottom compartment. The RIE and MW plasmas were generated at a frequency of 13.56 MHz and 2.45 GHz, respectively. Details of the sequential plasma activation can be found in [1]. Table 1 shows the plasma parameters used for surface activation and bonding of silicon wafers. The specimens of groups A and B show the plasma parameters to

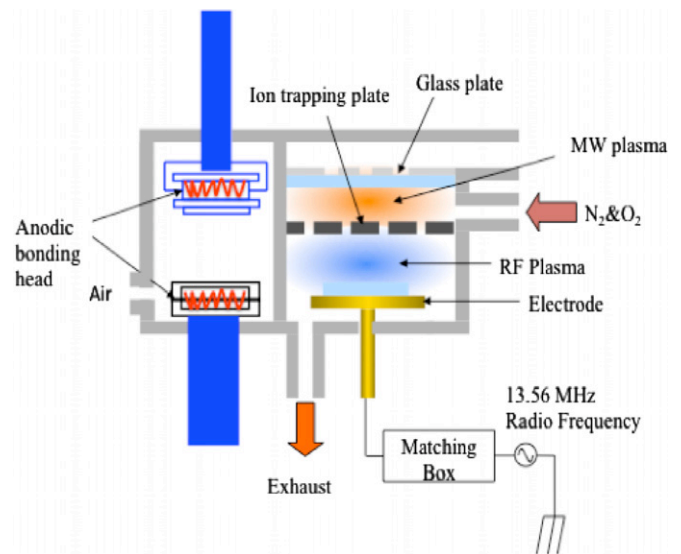


Figure 1. Schematic diagram of the hybrid plasma bonding (HPB) system used for the SPAB.

investigate the influence of O₂ RIE plasma time and power in the SPAB, respectively. The specimen C shows the O₂ RIE parameters for only O₂ RIE-activated bonding. After plasma activation, the wafers were taken out of the chamber and bonded together by applying pressure manually. Finally, the bonded specimens were cold-rolled under 0.2 MPa pressure at room temperature to remove trapped air. To investigate the influence of post-bonding annealing, the bonded specimens were annealed following a predefined annealing profile which will be discussed later in the paper. An IR transmission method was used to investigate the voids in the Si/Si bonded interface affected by different O₂ RIE times, powers and annealing temperatures.

For tensile strength measurements, the bonded specimens were diced into $10 \times 10 \text{ mm}^2$ pieces. The diced pieces were glued with copper jigs using standard Araldite adhesive from Huntsman Advanced Materials and the tensile strength was measured using the Instron tensile tester. Specimens for HRTEM were prepared from the bonded pairs by standard procedures including dicing, polishing, dimpling and ion-milling. To investigate the elemental composition at the bonded interface, EELS was performed. Two separate sets of specimens were prepared using the plasma parameters as shown in table 1 for contact angle and surface roughness

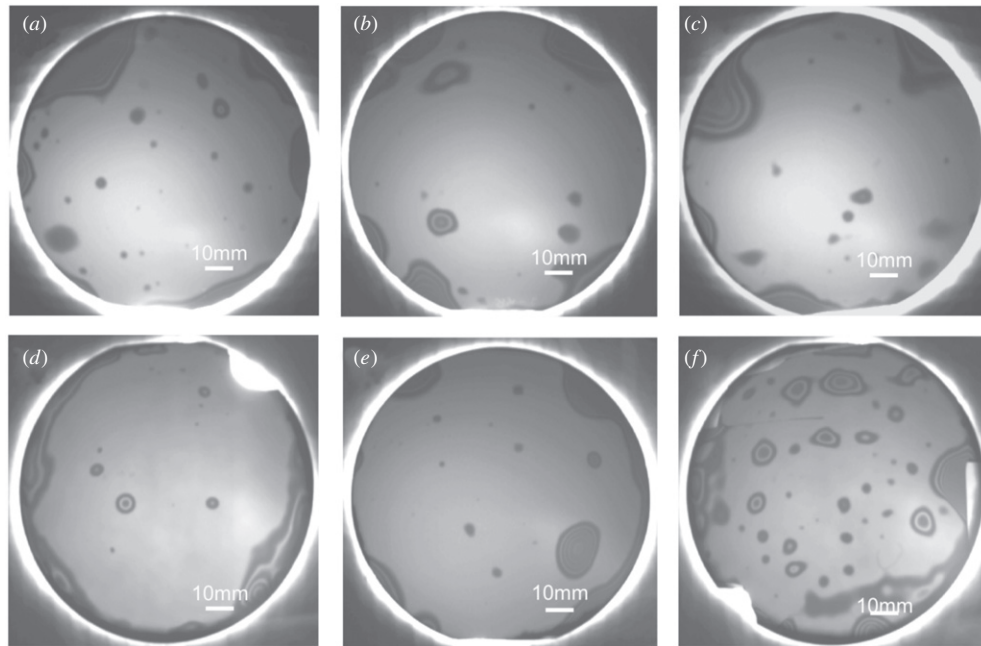


Figure 2. IR transmission images of Si/Si SPAB interfaces showing the influence of the O₂ RIE time (a) 15 s, (b) 30 s, (c) 60 s and power (d) 200 W, (e) 300 W and (f) 400 W on void formation without annealing.

measurements. The contact angle was measured using the sessile drop method with a deionized (DI) water droplet. The Kruss Drop Shape Analysis system (DSA100) was used to measure the contact angle 5 min after plasma activation. A contact angle below 2° cannot be detected using equipment. For surface roughness measurements, Veeco's Dimension Icon Atomic Force Microscope (AFM) was used.

3. Results and discussion

3.1. Plasma-induced void nucleation

Plasma treatment cleans and activates (i.e. forms new bonding sites) surfaces to achieve strong bonding strength at room temperature [6, 7]. However, the accelerated oxygen ions in the O₂ RIE plasma process damage the surface and increase the surface roughness resulting in the formation of voids [8, 9].

In general, voids form due to surface roughness, surface particles and residual particles on the surface caused by plasma bombardment. A smooth surface (rms roughness <0.5 nm) is required in order to avoid air-trapping-induced voids across the interface. While the voids due to surface particles can be controlled by the proper cleaning of the surface and use of particle-free bonding environment (e.g. clean room), the sequential plasma processing parameters such as O₂ RIE plasma time, power and gas pressure-induced voids can be detrimental to the quality of the bonded interface [9, 10]. In order to understand the role of plasma-induced nucleation of voids, IR transmission images for the SPAB Si/Si interfaces as a function of plasma processing parameters such as O₂ RIE plasma time and power were taken. As shown in figures 2(a), (b) and (c), no significant relationship between the O₂ RIE plasma time and the void formation in the SPAB

process was observed. On the other hand, the numbers of voids were increased rapidly with increasing O₂ RIE plasma power especially at 400 W, as shown in figure 2(f). A comparison between the influence of O₂ RIE time and power indicates that the O₂ RIE plasma power plays a dominant role in the formation of voids compared to O₂ RIE time.

3.2. Thermal-induced void nucleation

In order to investigate the nucleation behavior of voids, all the Si/Si bonded wafers (A1, A2, A3, B1, B2, B3 and C), as shown in table 1, were sequentially annealed up to 900 °C in air or nitrogen environments. Before annealing, the IR images were taken for all the specimens. Then, all the specimens were annealed at 200, 400, 600, 800 and 900 °C. The interfaces were observed after each annealing steps using an IR transmission camera. At all five temperatures the specimens were annealed for 4 h at a ramping rate of 200 °C h⁻¹. As a reference, the IR transmission images of non-activated Si/Si bonded interfaces are shown in figure 3. Since the surfaces were not treated with plasma, plasma-induced voids were not observed (figure 3(a)). A few particle-induced voids remained at the interface, which were not removed after annealing. A significant number of thermal voids were observed after annealing. The size of these voids increased with annealing temperature up to 800 °C, but their density decreased. Above 900 °C, the thermal-induced voids nearly disappeared. Figures 4 and 5 show the annealing-dependent void nucleation for only O₂ RIE-treated specimens (C) and SPAB specimen (B2), respectively.

The specimens were annealed up to 900 °C in nitrogen gas at a flow rate of 90 standard cubic centimeters per minute (sccm). In contrast to the non-activated reference Si/Si interface, the voids were not significantly changed up to

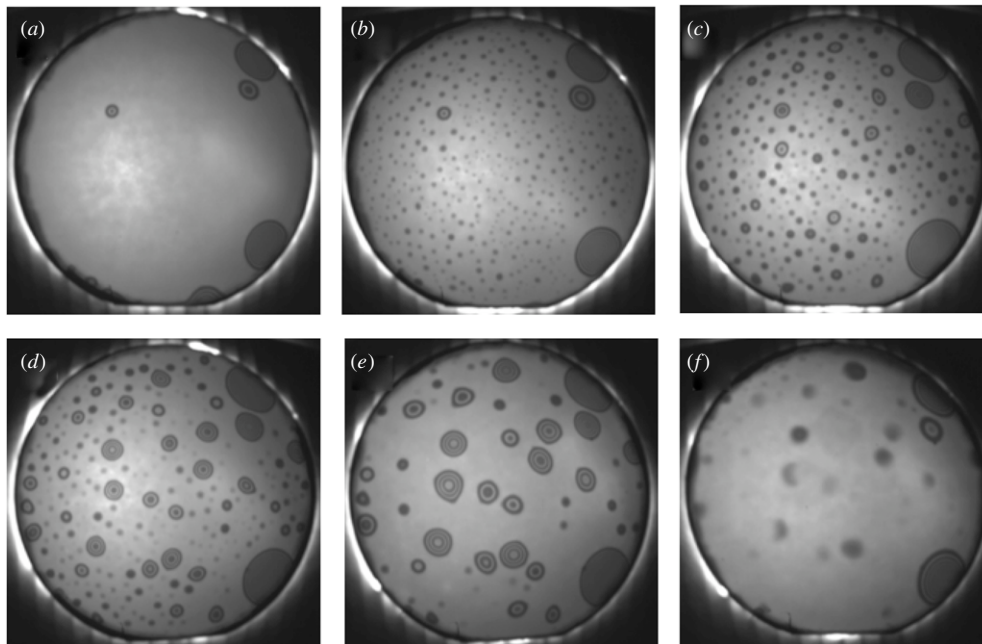


Figure 3. IR transmission images of nonactivated reference Si/Si interfaces (a) before (at room temperature) and after sequential annealing at (b) 200; (c) 400; (d) 600; (e) 800; (f) 900 °C in nitrogen ambient for 4 h in each step.

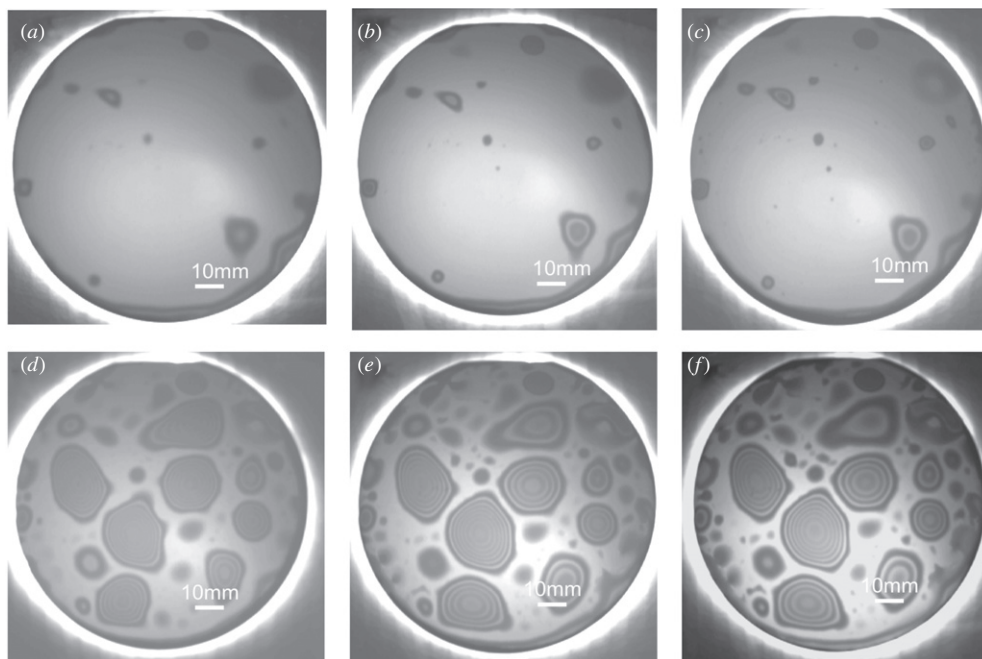


Figure 4. IR transmission images of O₂ RIE-treated silicon/silicon interfacial voids for specimen C (a) before (at room temperature), and after sequential annealing at (b) 200; (c) 400; (d) 600; (e) 800; (f) 900 °C in nitrogen ambient for 4 h in each step

400 °C both in the O₂ RIE and SPAB. From 600 °C annealing, unlike the non-activated Si/Si interface, new voids appear due to thermal annealing (now on termed as thermal voids) with the presence of the original voids due to plasma processing (termed as plasma voids). The size and shape of the voids at the SPAB interface (figure 5) were larger than those of the only O₂ RIE-processed interface (figure 4). In both cases, the size and shape of a few plasma voids were changed with a few Newton rings. The Newton rings result from the partial transmission

and reflection of light from the air–silicon interface at the unbonded regions [11].

The sizes of thermal voids were much bigger compared to those of the plasma voids. The nucleation of thermal voids is attributed to the generation of hydrogen gas from the oxidation reaction of silicon by the adsorbed water [12]. At 600 °C, perfectly bonded regions surrounded the thermal voids. No significant change of void evolutions was observed above 600 °C (figures 4–6) which contrasts to the non-activated

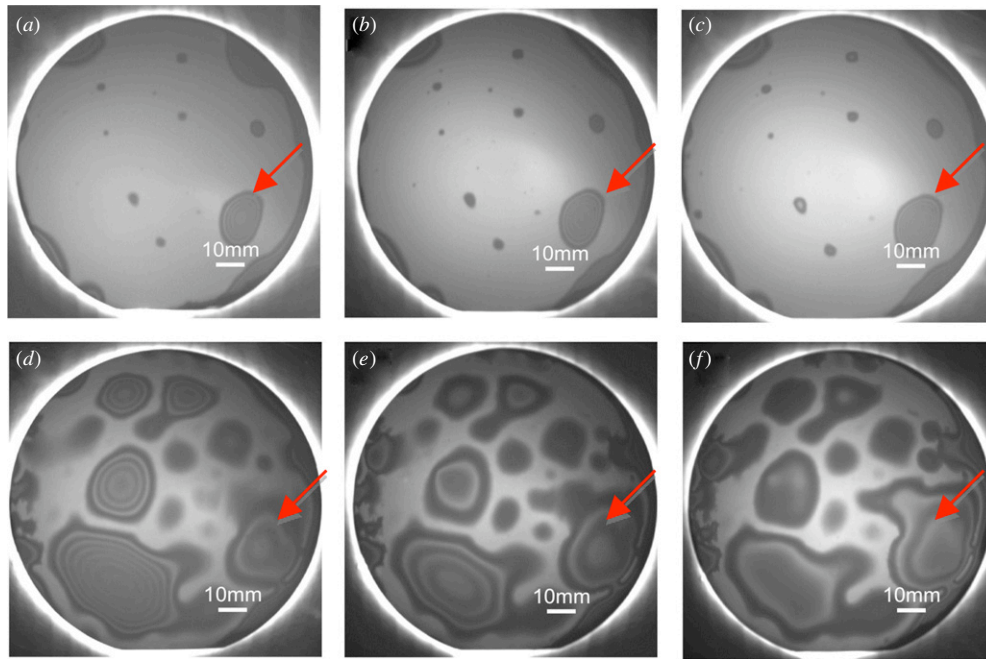


Figure 5. IR transmission images of SPAB treated Si/Si interfacial voids for specimen B2 (a) before and after sequential annealing at (b) 200; (c) 400; (d) 600; (e) 800; (f) 900 °C in nitrogen ambient for 4 h in each step.

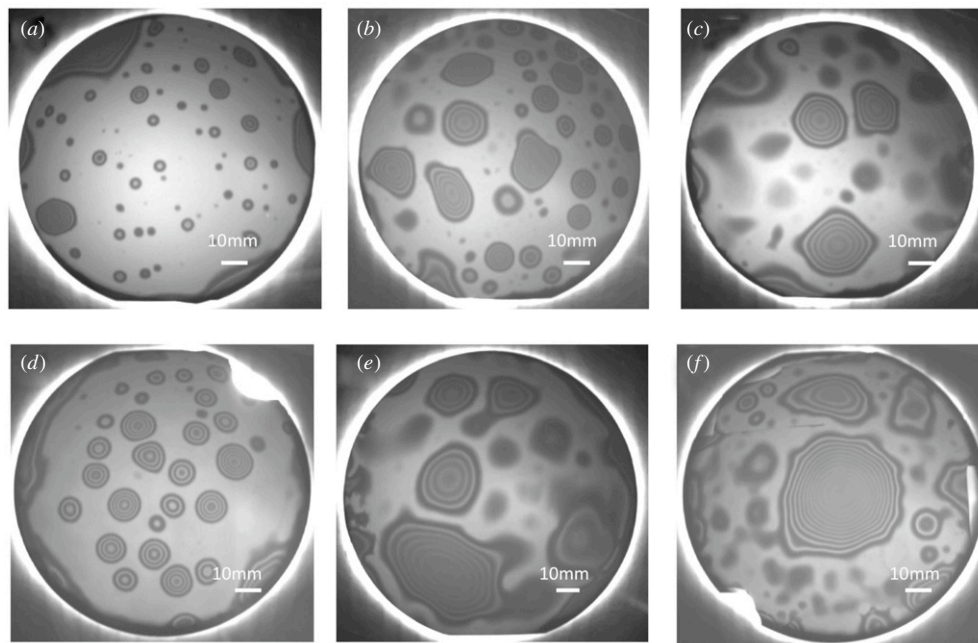


Figure 6. IR transmission images of all the specimens in groups A and B for transitions of void nucleation of the SPAB interfaces at (a) 15 s; (b) 30 s; (c) 60 s in air for 4 h at 600 °C and (d) 200 W; (e) 300 W; (f) 400 W (800 °C) in nitrogen ambient for 4 h at 600 °C.

interface (figure 3). Therefore, further annealing at higher temperatures neither generated voids nor changed the size and shape of the thermal voids. If one takes a look on the plasma-induced void (as indicated by arrows in figure 5) and its evolutions after annealing, one can detect a thermal void which is preferentially grown at the plasma-induced defect site. A comparison of the IR images at 600 (figure 5(d)), 800 (figure 5(e)) and 900 °C (figure 5(f)) indicates that once the size and shape of the voids are defined at 600 °C,

they cannot be changed by thermal viscous flow because of high bonding strength at the surrounding area of the voids already formed at 600 °C. The larger size of the bubbles in the SPAB compared to that of the O₂ RIE-processed interface is attributed to the presence of N₂ radicals in the SPAB. The N₂ radicals produce highly reactive surfaces [2]. The high chemical reactivity of the sequential plasma-treated surfaces may adsorb higher amount of water molecules before bonding than that of the O₂ RIE plasma-activated surfaces, resulting

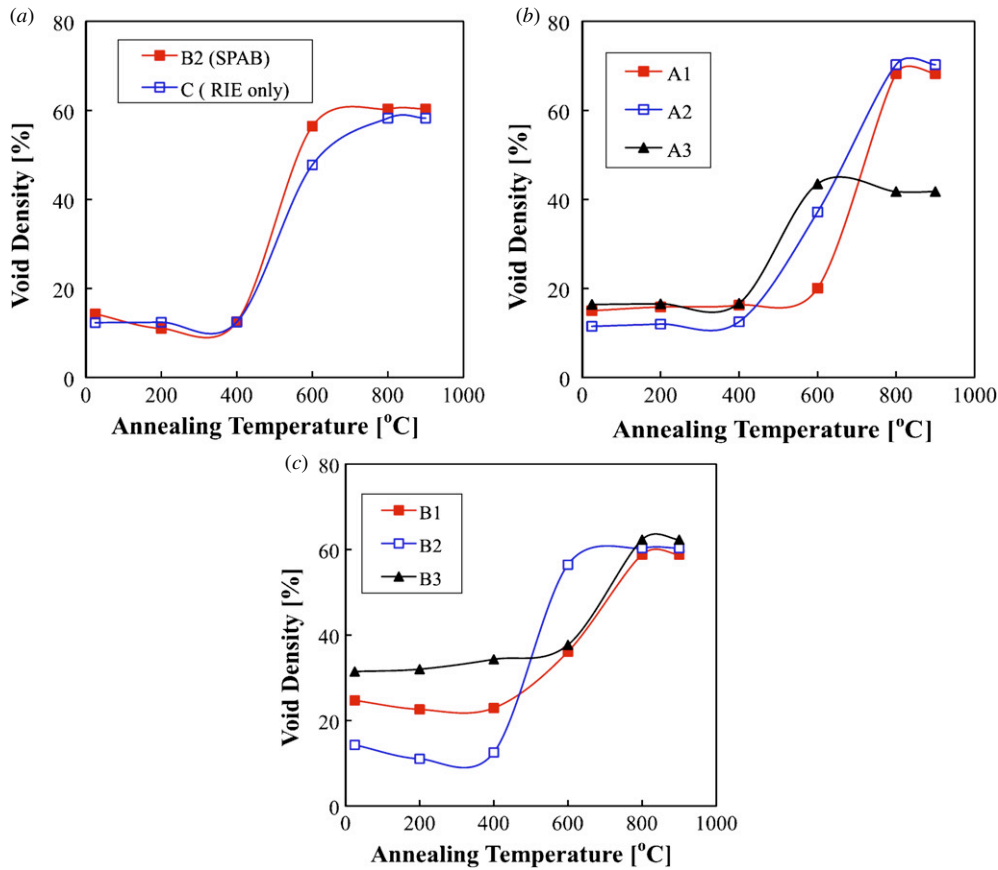


Figure 7. (a) SPAB specimen (B2) compared with the only RIE-bonded specimen (C) annealed in nitrogen gas, (b) O₂ RIE time-dependent specimens (A1, A2, A3) annealed in air, and (c) O₂ RIE power-dependent specimens (B1, B2, B3) annealed in nitrogen gas for 4 h at each annealing step.

in more H₂ at the interface from silicon oxidation and hence larger voids.

As previously seen, the thermal voids were grown preferentially at plasma-induced defect sites on the activated surfaces. Therefore, the investigation of the void nucleation associated with their transitions (i.e. abrupt changes) offers insight into the size and shape of the nucleated voids. Figure 6 shows the transitions of thermally nucleated voids at the SPAB interfaces as a function of O₂ RIE time and power at 600 °C. Due to the dominant role of O₂ RIE power in the void formation (as shown in figure 2(f)) in the SPAB, the dependence of the voids formation on the O₂ RIE power was investigated after annealing the specimens in the inert media using nitrogen gas. On the other hand, the O₂ RIE time-treated specimens were annealed in air to see the environmental influence on the bonded interface. The transitions of the void nucleation for all the specimens regardless of RIE time and power occurred at 600 °C except for the specimen treated with 400 W O₂ RIE. For the specimen treated with 400 W O₂ RIE, the transition of the void nucleation was occurred at 800 °C. The results indicate that viscous flow of oxides is required for the transition of voids. Viscous flow of oxides occurs only when there is excess gas, which cannot be accommodated (i.e. trapped) at the defect sites. Therefore, the transition of voids for the specimen treated with 400 W O₂ RIE did not occur at 600 °C due to existence of enough open space to accommodate

the gas at the interface. The temperature-dependent void evolution showed that the size of the thermal voids increased with the increase in O₂ RIE power and time.

Figure 7 shows the quantitative analysis of the void density of (a) the SPAB specimen (B2) compared with the only RIE-bonded specimen (C) annealed in nitrogen gas, (b) O₂ RIE time-dependent specimens (A1, A2, A3) annealed in air, and (c) O₂ RIE power-dependent specimens (B1, B2, B3) annealed in nitrogen gas as a function of annealing temperatures. The void density was estimated from the IR images on scaled paper. A few percents of discrepancy may exist in the estimation of the void density due to human errors. From figure 7(a), no significant change in the void density was observed between the O₂ RIE-bonded and SPAB interfaces. On the other hand, the O₂ RIE time- (figure 7(b)) and power-dependent (figure 7(c)) behavior of the void density in the SPAB interfaces showed that the plasma void density remained constant up to 400 °C, and the thermal void density suddenly increased for all the specimens at 600 °C except for the specimen (B3) treated with an O₂ RIE power of 400 W in nitrogen. For specimen B3, thermal void nucleation started at 800 °C. Below 400 °C, the void density for the specimens (figure 7(c)) annealed in N₂ gas was higher than that of the specimens (figure 7(b)) annealed in air. Further research is needed to clarify the role of annealing environment on the nucleation of voids. Above 600 °C, the amount of thermal voids density for specimen A2 was higher

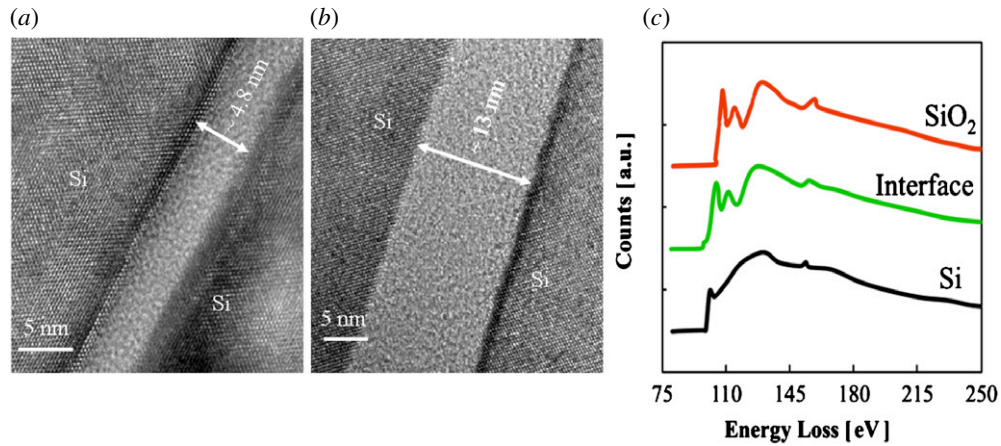


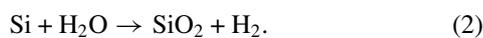
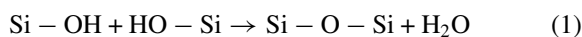
Figure 8. HRTEM images of Si/Si sequential plasma-activated bonded interfaces of the specimen (a) before annealing, (b) after annealing at 600 °C and (c) compositional distribution by EELS analysis after annealing at 600 °C.

compared to that of specimen B1. This higher amount of void density was caused by higher activation time of the N₂ radical (30 s) for specimen A2. The O₂ RIE plasma activation time for A1 and A2 were 15 and 30 s respectively that were not sufficient to remove native oxides and surface particles from the silicon surface. This remaining native oxides and surface particles worked as a precursor for the enlargement of the voids. On the other hand, specimen A3 treated for 60 s had lower saturated void density at and above 600 °C. This is attributed to the better removal of native oxides and surface particles due to the prolonged surface activation. In addition, it has been reported that plasma activation not only removes native oxides but also deposits an oxide layer on the treated surface [13]. This plasma-induced oxide layer (which grows with activation time) helps absorb the reaction byproduct at the interface and thus reduces void density [14].

3.3. Microstructural investigation

In order to correlate the transitions of macro-scale voids with the nanometer scale interfacial behavior, the HRTEM was performed before and after sequentially annealing (as mentioned before) the bonded specimen at 600 °C as shown in figures 8(a) and (b), respectively.

The HRTEM images show a nanometer thick amorphous layer at the bonded interface. The amorphous layer thickness of ~4.8 nm before annealing enlarged to ~13 nm after sequential annealing at 600 °C. This abrupt change in amorphous layer thickness can be correlated to the oxidation of silicon (reaction (2)) by the water adsorbed onto the plasma-activated silicon surfaces and produced from reaction (1), as follows [15]:



Therefore, the reaction product SiO₂ is responsible for the abrupt change in amorphous layer thickness and reaction byproduct H₂ is responsible for the nucleation of thermal voids across the interface at 600 °C.

To investigate the elemental composition at the bonded interface after annealing, EELS was performed with the specimen shown in figure 8(b). The EELS experiment was performed using a field-emission TEM (JEOL 2100F, Cs = 0.50 mm) in conjunction with a Gatan Enfina 1000 spectrometer, operating at 200 kV. The energy resolution was about 1.0 eV and a 1.0 nm diameter probe was used. Core-loss EELS spectra of N–K, Si–L_{2,3} and O–K were recorded. From the EELS spectra no nitrogen was detected at the bonded interface. The Si–L_{2,3} edges at 125–175 eV and the O–K edges at 540–560 eV were observed at the amorphous interface layer. To investigate the characteristic behavior of the amorphous interface layer, the Si–L_{2,3} edges of the amorphous interface layer were compared with those of standard Si and SiO₂ as shown in figure 8(c). The Si–L_{2,3} edges from the amorphous interface layer were identical to those of the standard SiO₂. Thus, the presence of SiO₂ at the interface and hence the oxidation of silicon was confirmed.

3.4. Tensile strength and hydrophilicity

Figures 9(a) and (b) show the tensile strength of SPAB Si/Si specimens that sequentially annealed up to 900 °C as a function of O₂ RIE time and power, respectively, compared with that of the non-activated Si/Si interface. The bonding strength increased with the increase of O₂ RIE time. The rapid increase in tensile strength from 30 s to 60 s O₂ RIE time is attributed to the reduction in void density as shown in figure 7(b) (compare A2 and A3). Highest standard deviation in the tensile strength was observed for 60 s of O₂ RIE activation, which is due to the accumulation of voids resulting in larger voids.

The bonding strength decreased with the increase of O₂ RIE power as shown in figure 9(b). The standard deviations were almost identical for different O₂ RIE powers. A single data point for the bonding strength of only O₂ RIE processed (specimen C) at 300 W is also included for comparison. The bonding strength of Si/Si at different O₂ RIE powers was lower than that at different O₂ RIE times. This difference is due to the discrepant MW N₂ radical's time, as discussed below in the comparison with contact angles. It is important to note

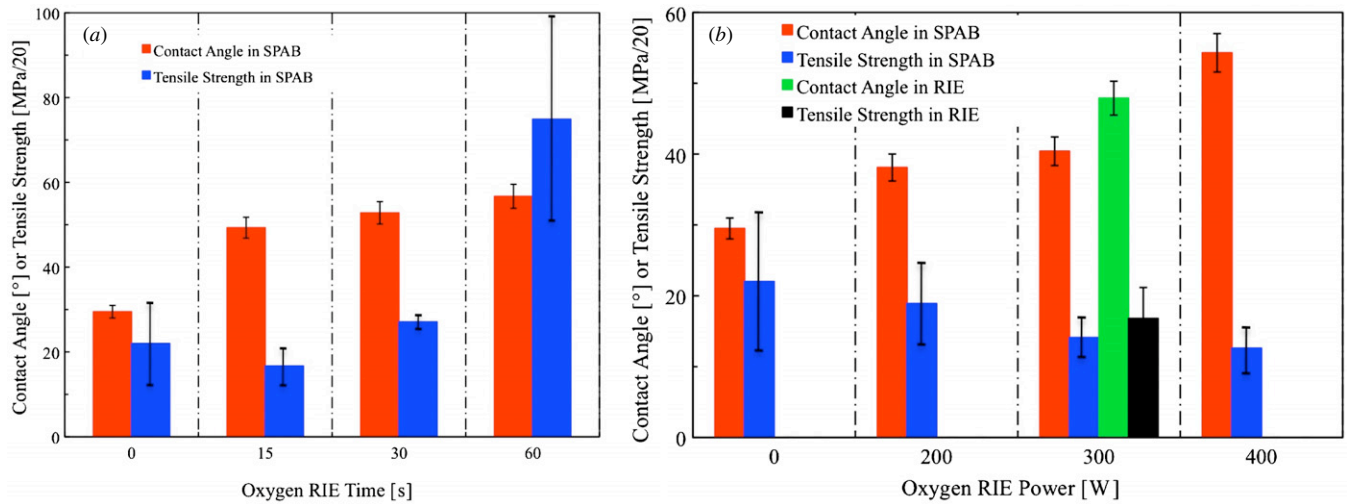


Figure 9. Tensile strengths of Si/Si SPAB interface at 900 °C versus (a) O₂ RIE time and (b) O₂ RIE power compared with contact angles of silicon at room temperature.

that, after the tensile pulling test, the wafers were debonded from the interface. Therefore, the bulk fracture of Si was not observed.

To investigate the change in tensile strength with different O₂ RIE times and powers, contact angle measurements were performed. Figures 9(a) and (b) also show the contact angle of a droplet of DI water on the silicon wafer surface with different O₂ RIE activation times and powers compared with that of the non-activated specimen. The contact angles were increased with the increase in O₂ RIE time and power. The increase in O₂ RIE time and power results in an increase in surface roughness as discussed later in the paper, caused by physical bombardment of plasma. The contact angle of the rough surface is higher than that of the smooth surface [16]. Hence, the increase in the contact angle is attributed to the increase in surface roughness with O₂ RIE time and power.

An increase in the contact angle refers to a decrease in surface hydrophilicity. In general, the decrease in hydrophilicity results in a decrease in surface energy [17] and hence a decrease in bonding strength without annealing [18]. However, after sequential annealing up to 900 °C, an increase in the bonding strength was observed with the increase of O₂ RIE activation time, as shown in figure 9(a). In fact, the sequentially treated silicon surface is passivated by O_xN_y layers [1]. With increasing annealing temperatures, these O_xN_y layers decompose. Therefore, the bonding strength at 900 °C was increased with the increase in the water contact angle as a function of O₂ RIE time.

On the other hand, when the O₂ RIE power was varied, an abrupt increase in the contact angle was observed from 300 W to 400 W. This increase attributes to higher surface roughness (discussed later in the paper) caused by strong bombardment at 400 W. This increased surface roughness resulted in an abrupt increase in void density from 300 W to 400 W as shown in figures 2(e)–(f). However, after sequential annealing up to 900 °C, the tensile strength was smoothly reduced from 300 W to 400 W as shown in figure 9(b). In contrast to the O₂ RIE time-dependent behavior, the decrease in the tensile

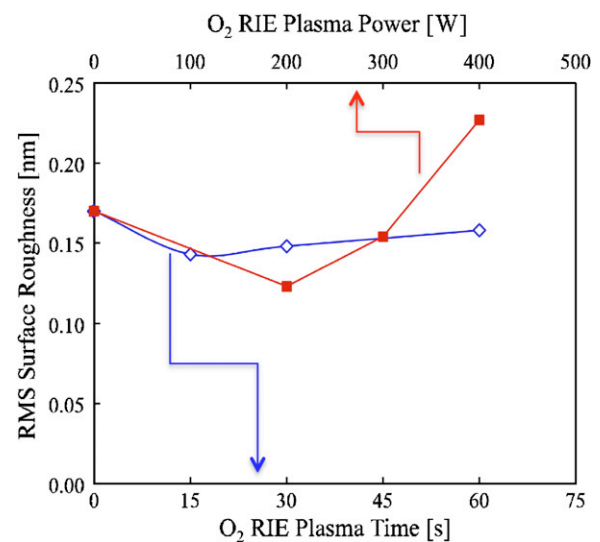


Figure 10. Surface roughness of silicon as a function of O₂ RIE plasma time and power in the SPAB.

strength as a function of O₂ RIE power can be attributed to the increase in the contact angle.

A comparative study of contact angles as shown in figures 9(a) and (b) for specimens A2 and B1 shown in table 1 reveals that a change in N₂ MW time from 15 s to 30 s changes the contact angle from 38.1 to 52.8° and the bonding strength from 0.95 MPa to 1.37 MPa with other parameter constants. Hence, a dominant role of MW N₂ radical's time was observed when increasing the bonding strength. The issue remained is why the bonding strength reduced with the increase in the O₂ RIE power, which can be explained using the surface roughness investigation.

3.5. Role of surface roughness on bonding performance

Figure 10 shows the dependence of the surface roughness of silicon on the O₂ RIE time and power in the sequential

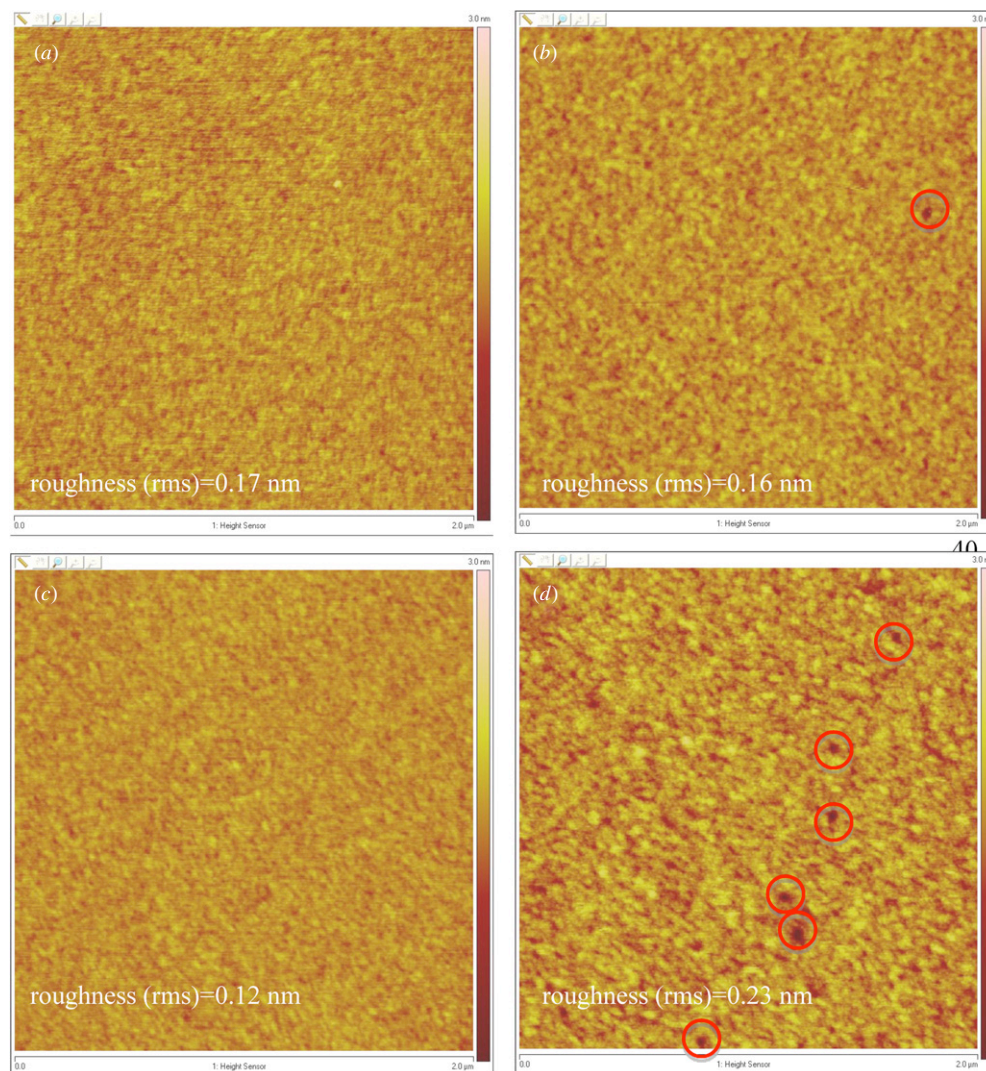


Figure 11. Atomic force microscopy (AFM) images of the silicon surface (a) before, (b) after O₂ RIE activation with 300 W for 30 s (specimen C), (c) after O₂ RIE activation with 200 W for 30 s followed by N₂ MW radicals activation with 2500 W for 30 s (specimen B1), and (d) after O₂ RIE activation with 400 W for 30 s followed by N₂ MW radicals activation with 2500 W for 15 s (specimen B3).

activation. The rms roughness was measured in tapping mode over a scanning area of $2 \times 2 \mu\text{m}^2$ using an atomic force microscope. The measurements were repeated three times and reproducible surface roughness was achieved. Before activation, the rms surface roughness was 0.17 nm. After 15 s O₂ RIE activation, the rms roughness decreased to 0.14 nm. A further increase in activation time resulted in an increase in roughness, but still lower than that of before activation even after activation for 60 s.

As can be seen from figure 10, the surface roughness also increased with the increase in O₂ RIE power. However, the rate of increase in the surface roughness with the increase in the O₂ RIE power is high compared to the O₂ RIE time. The slopes for the surface roughness curves differ, indicating different etching behaviors of O₂ RIE time and power. While a smooth surface (roughness 0.12 nm) was observed at 200 W, it was rough (roughness 0.23 nm) at 400 W. The increased surface roughness at 400 W is responsible for the increased void nucleation (figure 2(f)) as well as for the severe degradation of bonding strength at 400 W (figure 9(b)).

This result is in agreement with previous studies [19], where bonding energy was correlated with surface roughness. In order to find the relationship between interfacial voids and surface roughness, a comparative view on the surface roughness is given in figure 11. It includes the images of the silicon surface (a) before activation, and after activation under processing conditions for specimens (b) C, (c) B1, and (d) B3. The AFM images show that the silicon surface becomes smooth after activation (compare figures 11(a) and (c)).

With the increase in the activation power from 200 (figure 11(c)) to 300 W (figure 11(b)), the surface roughness increased. This trend is continued. In fact, the increase in plasma power fortifies the physical bombardment process of ionized particles. Once the surface is free from native oxides, particles and contaminations, the energetic ionized particles start digging the surface and create nano-defects such as nanopores and craters on the surface. In particular, there were a significant number of such defects present on the whole surface of the specimen treated with 400 W O₂ RIE. Red circles on the images indicate some nanopores. The estimated

depth of the nanopores was as high as 2.2 nm. This finding confirmed porosity on the activated surfaces of silicon, which was assumed in [4, 20]. The nanopores and craters were acted as trapping sites for the gas at the bonded interface. Annealing at high temperature does not remove these defect sites. Viscous oxides fill the defect sites. Sequential annealing causes brittle oxides, which are higher at the defect sites. Therefore, the bonding strength at 900 °C decreased with the increase in the O₂ RIE power due to the increased surface roughness and defects.

4. Conclusions

Void nucleation at sequentially plasma-activated Si/Si bonded interface has been systematically investigated to explore the reliability of SPAB at high temperature. The experiments show that O₂ RIE plasma power played a dominant role on void nucleation over the O₂ RIE time. A strong relationship between bonding strength and voids was observed after annealing. The nucleation of thermal voids for all specimens regardless of O₂ RIE time and power occurred at 600 °C except for the specimen treated with 400 W O₂ RIE which was appeared at 800 °C. Thermal void nucleation was preferentially at the plasma-induced defect sites. The abrupt increase in void density at 600 °C is correlated to the abrupt increase in interfacial amorphous layer thickness at 600 °C. EELS confirmed the presence of silicon oxide at the bonded interface. The bonding strength (after annealing at 900 °C) increased and decreased with the increase in the O₂ RIE activation time and power, respectively. The contact angle and roughness of the sequentially plasma-treated surfaces were studied to explain the void nucleation and reduction of the bonding strength. The plasma-induced defect sites such as nanopores and craters were responsible for the severe reduction of bonding strength for the specimens treated relatively with high power (i.e. 400 W).

Acknowledgments

This research was supported by a discovery grant (no. 327947) from the Natural Science and Engineering Research Council of Canada and an infrastructure grant (no. 12128)

from the Canada Foundation for Innovation (CFI). Professor Jamal Deen is greatly thanked for his support and assistance in establishing nanobonding and interconnection research at the Micro- and Nano-Systems Laboratory at McMaster University. The authors acknowledge Professor T Suga for the development of the sequentially plasma-activated bonding method. Professor Moon J Kim is acknowledged for the contribution to the high-resolution transmission electron microscopy.

References

- [1] Howlader M M R, Suehara S, Takagi H, Kim T H, Maeda R and Suga T 2006 *IEEE Trans. Adv. Packag.* **29** 446
- [2] Kibria M G, Zhang F, Lee T H, Kim M J and Howlader M M R 2010 *Nanotechnology* **21** 134011
- [3] Bruel M 1996 *Nucl. Instrum. Methods Phys. Res. B* **108** 313
- [4] Howlader M M R, Suga T, Itoh H, Lee T H and Kim M J 2009 *J. Electrochem. Soc.* **156** H846
- [5] Howlader M M R, Itoh H, Suga T and Kim M J 2006 *ECS Trans.* **3** 191
- [6] Bengtsson S and Amirfeiz P 2000 *J. Electron. Mater.* **29** 909
- [7] Dragoi V, Mittendorfer G, Thanner C and Lindner P 2008 *Microsyst. Technol.* **14** 509
- [8] Weinert A, Amirfeiz P and Bengtsson S 2001 *Sensors Actuators A* **92** 214
- [9] Zhang X X and Raskin J-P 2005 *J. Microelectromech. Syst.* **14** 368
- [10] Ma X, Liu W, Song Z, Li W and Lin C 2007 *J. Vac. Sci. Technol. B* **25** 229
- [11] Horn G, Gabriel M, Lesniak J and Mackin T J 2009 *J. Electrochem. Soc.* **156** 27
- [12] Toyoda E, Sakai A, Isogai H, Senda T, Izunome K, Nakatsuka O, Ogawa M and Zaima S 2009 *Japan J. Appl. Phys.* **48** 011202
- [13] Pasquariello D, Hedlund C and Hjort K 2000 *J. Electrochem. Soc.* **147** 2699
- [14] Mitani K and Gosele U M 1992 *Appl. Phys. A* **54** 543–52
- [15] Ventosa C, Rieutord F, Libralesso L, Morales C, Fournel F and Moriceau H 2008 *J. Appl. Phys.* **104** 12
- [16] Yang C, Tartaglino U and Persson B N J 2006 *Phys. Rev. Lett.* **97** 116103
- [17] Ma X, Chen C, Liu W, Liu X, Du X, Song Z and Lin C 2009 *J. Electrochem. Soc.* **156** H307
- [18] Bhattacharya S, Datta A, Berg J M and Gangopadhyay S 2005 *J. Microelectromech. Syst.* **14** 590
- [19] Miki N and Spearing S M 2003 *J. Appl. Phys.* **94** 6800
- [20] Sanz-Vealsco A, Amirfeiz P, Bengtsson S and Colinge C 2003 *J. Electrochem. Soc.* **150** G155